Density Functional Theory and Quantitative Structure-Activity Relationship Studies of some Quinoxaline derivatives as potential Corrosion Inhibitors for Copper in Acidic Medium

Mwadham M. Kabanda[*]*, Eno E. Ebenso*

Department of Chemistry, School of Mathematical & Physical Sciences, North-West University (Mafikeng Campus), Private Bag X2046, Mmabatho 2735, South Africa.
[*]E-mail: mbyechura@gmail.com

Density Functional Theory (DFT) using the B3LYP functional and Quantitative Structure-Activity Relationship QSAR studies is reported on some quinoxaline derivatives namely 3-methyl-2-phenyl quinoxaline (MPQ), 2,3-diphenyl quinoxaline (PPQ), 3-methyl-2(2-hydroxyphenyl)quinoxaline (MHPQ), 3-phenyl-2(2-hydroxyphenyl)quinoxaline (PHPQ) and 3-methyl-2(3-methoxy,4-hydroxyphenyl)quinoxaline (MM_tHPQ) used as corrosion inhibitors for copper in acidic medium. DFT was utilized to model the quinoxaline···Cu interaction mechanism in order to obtain molecular reactivity parameters (for elucidating the reactivity tendency for each of the studied quinoxaline derivative). Some of the reactivity parameters were correlated with the experimentally determined inhibition efficiencies using quantitative structure activity relationship (QSAR). The results show that an optimum of three quantum chemical parameters is sufficient to correlate with experimentally determined inhibition efficiencies. The quinoxaline···Cu interaction shows that the Cu atom binds to the quinoxaline derivatives with the preferred geometries corresponding to cases in which the Cu atom is in a multi-dentate mode or geometry.

1. INTRODUCTION

Metal dissolution is a major industrial challenge because of the wide industrial applicability of metal-made products such as reaction vessels in chemical industries, pipelines for fluid transportation, machinery, chemical battery, etc. Metal dissolution may result in high productivity loss arising from the malfunctioning of the corroded instruments and contamination of main industrial products (e.g.,

chemical products) by the aqueous corrosion products. Several approaches have been used to prevent metal dissolution and thereby lengthen the working time of metal-made products for industrial utilizations. Among these approaches is the use of corrosion inhibitors which, when applied in small quantity, adsorb on the metal surface and thereby block the interaction between the metal surface and the corrosive medium [1, 2]. The effectiveness of corrosion inhibitors is highly determined by their physicochemical properties (e.g., electron density, geometric factors, molecular volume, etc.,) while the adsorption onto the metal surface is determined by the type of the metal, the nature of the inhibitor and the electrochemical potential at the metal-solution interface [2]. Therefore, a comparison of the physicochemical properties of compounds that have corrosion inhibition potential assists largely in the selection of compounds with good corrosion inhibition efficiency, which could be synthesized and their inhibition efficiency determined experimentally. The physicochemical properties of molecules are efficiently studied by utilizing quantum chemical methods. These methods are finding wide applicability in the investigation of compounds with promising corrosion inhibition potential less time consuming and because they are economically less expensive as compared to experimental techniques. Quantum chemical methods are also increasingly being utilized in the elucidation of the interaction mechanism between corrosion inhibitor molecules and the metal surface [3].

The objective of this article is to compare and determine trends in the molecular reactivity and selectivity parameters for selected quinoxaline derivatives and to correlate some of the quantum chemical parameters with the experimental determined inhibition efficiency (%IE) using quantitative structure activity relationship (QSAR). The study also intends to investigate the interaction mechanism between each quinoxaline and a single Cu atom, as a prototype for Cu surfaces, to determine the preferred complexes, preferred binding sites of the Cu atom and the mode of charge transfer. The studied quinoxaline derivatives namely 3-methyl-2-phenyl quinoxaline (MPQ), 2,3-diphenyl quinoxaline (PPQ), 3-methyl-2(2-hydroxyphenyl)quinoxaline (MHPQ), 3-phenyl-2(2-hydroxyphenyl)quinoxaline (PHPQ) and 3-methyl-2(3-methoxy,4-hydroxyphenyl)quinoxaline (MM$_t$HPQ).are shown in figure 1. The presence of heteroatoms in all the selected quinoxaline derivatives suggests that in aqueous acidic media, the inhibitors are likely to be protonated. To this effect, the study takes into consideration both the neutral and the protonated species to determine the preferred species (of the inhibitors) to interact with the metal surface. Moreover, the study is conducted *in vacuo* and in water solution because of the importance of aqueous media in electrochemical reactions.

These compounds have already been shown through experimental studies to have high corrosion inhibition efficiencies for copper in nitric acid, with the order of inhibition efficiency being MM$_t$HPQ > PPQ > MPQ > PHPQ > MHPQ [4].

MPQ   **PPQ**   **MHPQ**
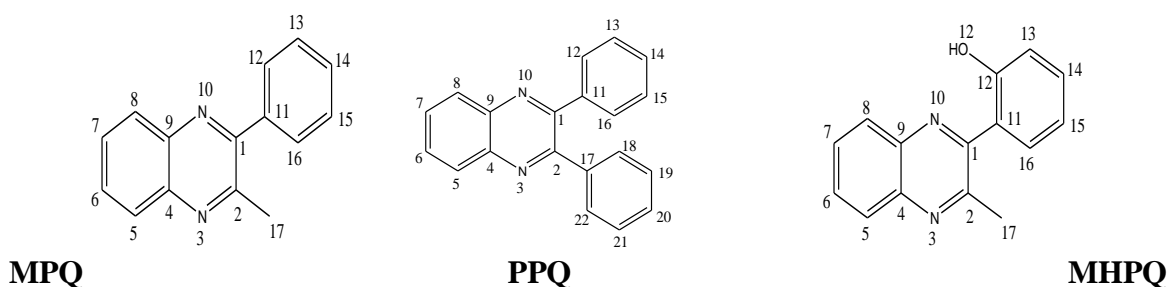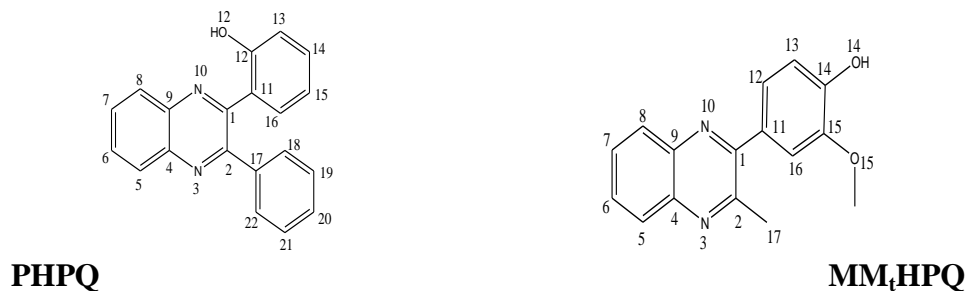
Figure 1. Schematic representation and the atom numbering for studied quinoxaline derivatives.

2. COMPUTATIONAL DETAILS

All geometry optimizations were performed by utilizing the density functional theory (DFT) at the B3LYP functional (Becke's Three Parameter Hybrid Functional using the Lee-Yang-Parr correlation functional [5]). Calculations *in vacuo* were performed by utilizing the 6-31G(d), 6-31+(d) and 6-311(d) basis sets to compare the effects of different basis sets on the electronic properties of the systems. Among the chemical descriptors for which DFT/B3LYP provides good description include the energy of the highest occupied molecular orbital (E_{HOMO}), the energy of the lowest unoccupied molecular orbital (E_{LUMO}) and related properties such as polarizability, hardness and electronegativity [6]. These quantities are better discussed in terms of the Koopman's theorem [7, 8]; Electronegativity (χ) is the measure of the power of an electron or group of atoms to attract electrons towards itself [9]:

$$\chi \cong -\tfrac{1}{2}\,(E_{HOMO} + E_{LUMO}) \tag{1}$$

Chemical hardness (η) measures the resistance of an atom to charge transfer [10]:

$$\eta \cong -\tfrac{1}{2}\,(E_{HOMO} - E_{LUMO}) \tag{2}$$

Global softness (σ), describes the capacity of an atom or group of atoms to receive electrons [10]:

$$\sigma = 1/\eta \cong -2/(E_{HOMO} - E_{LUMO}) \tag{3}$$

The proton affinity (PA) value was estimated using the equation.

$$PA = E_{prot} + E_{H2O} - E_{non\text{-}prot} + - E_{H3O+} \tag{4}$$

where E_{prot} and $E_{non\text{-}prot}$ are the total energies of the protonated and the non-protonated (neutral) inhibitors respectively, E_{H2O} is the total energy of a water molecule and E_{H3O+} is the total energy of the hydronium ion.

The calculations for the complexes were performed using the B3LYP/6-31G(d) because it provides fair estimate of the binding energies involving Cu [11]. The interaction energy between the inhibitor and the Cu atom was estimated using the equation;

$$E_{inter} = E_{inhibitor \cdots Cu} - E_{Cu} - E_{inhibitor} \qquad (5)$$

where $E_{inhibitor \cdots Cu}$ is the total energy of the optimized complex, E_{Cu} is the total energy of the isolated Cu and $E_{inhibitor}$ is the total energy of the isolated inhibitor. The greater the computed value, the stronger is the affinity of copper atom to bind to the inhibitor molecule. However, because of geometry flexibility of the quinoxaline derivatives, it is necessary to estimate the deformation energy (i.e., energy due to changes in the geometry of the inhibitor on complexation with Cu) and subtract it from the E_{inter} in order to obtain the binding energy (E_b) between the inhibitor and the Cu atom. The deformation energy was estimated as the energy difference between the total energy of the inhibitor in the complex ($E_{i, comp}$) and the total energy of the corresponding isolated optimized inhibitor molecule (E_{i-opt}), i.e.,

$$E_{def} = E_{i,comp} - E_{i \, opt} \qquad (6)$$

where $E_{i, comp}$ is estimated by running a single point calculation on the geometry of the inhibitor in the complex molecule. In this way, the inhibitor-metal binding energy (E_b) is estimated as the energy difference between the interaction energy and the deformation energy

$$E_b = E_{inter} - E_{def} \qquad (7)$$

All calculations were performed by utilizing the Spartan 10 V1.01 program [12]. Calculations in water solution were performed by utilizing the SM8 model [13]. Schematic structures were drawn using the ChemOffice package in the UltraChem 2010 version and the optimized structures were drawn using the Spartan 10 V1.01 program.

3. RESULTS AND DISCUSSION

3.1. Reactivity parameters

The optimized geometries of the studied quinoxaline derivatives and their protonated species are shown in figure. 2 while the HOMO and the LUMO together with their corresponding densities are presented in figure. 3. These molecular orbitals have a crucial role in determining the reactivity of molecules and have direct influence in the adsorption of the inhibitors onto the metal surface [14]. The regions of the molecule on which the HOMO is distributed indicate the sites which have the highest tendency to interact with the metal surface. In MPQ, the HOMO is delocalized throughout the three rings but has maxima on C6, C12 and C13; in PPQ, the HOMO is delocalized throughout the molecule

with maxima on C1-C2, C6–C7, C4–C9, C11–C12, C13–C14 and C20–C21 regions; in MHPQ, PHPQ and MM$_t$HPQ, the HOMO is only localized on the ring at C1 and has maxima on C11−C12 and C15−C16 regions.

The LUMO indicates regions which have the highest tendency to accept electrons. In the investigated quinoxaline derivatives, the LUMO is spread only on the quinoxaline moiety and has an anti-bonding character on N atoms. The LUMO density suggests that the

a)   Neutral species of the quinoxaline derivatives

MPQ   PPQ   MHPQ

PHPQ   MM$_t$HPQ

b)   Protonated species of the quinoxaline derivatives

MPQ   PPQ   MHPQ

PHPQ   MM$_t$HPQ
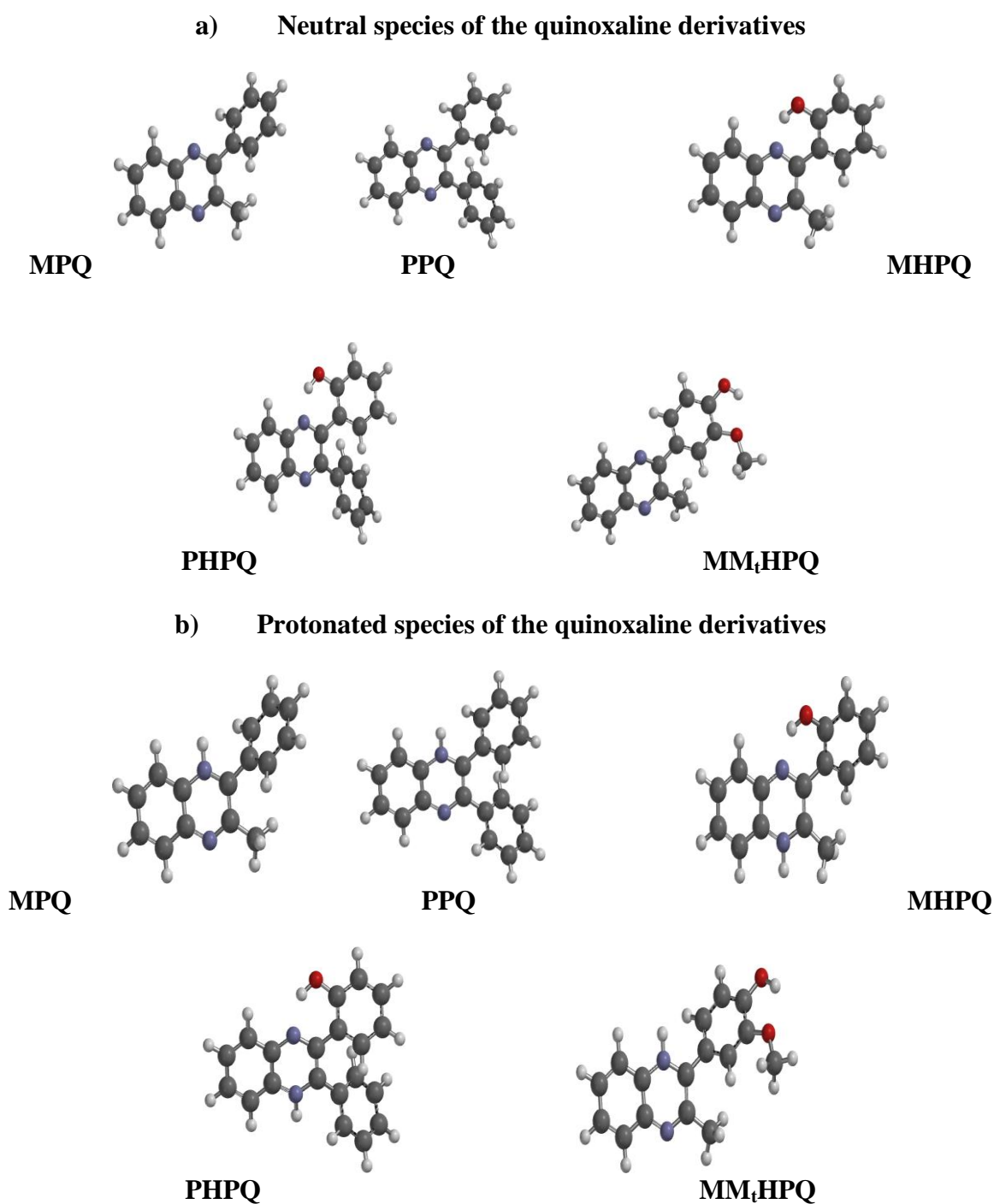
Figure 2. Optimized lowest energy conformers of the neutral (a) and protonated species of the studied quinoxaline derivatives. B3LYP/6-31G(d,p results *in vacuo*.

MPQ	PPQ	MHPQ	PHPQ	MM$_t$HPQ

HOMO

HOMO density
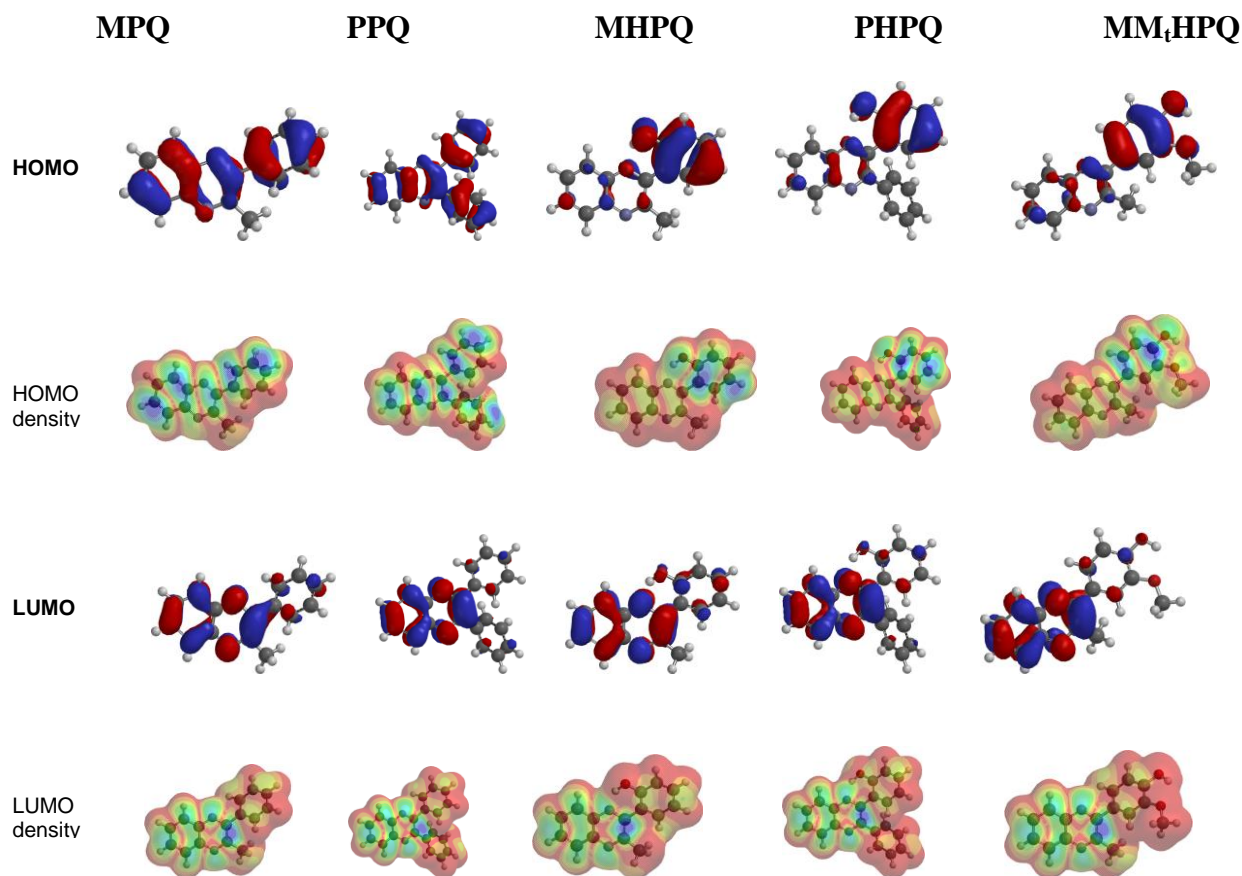
LUMO

LUMO density

Figure 3. The HOMO, the LUMO and the corresponding densities for the studied quinoxaline derivatives (B3LYP/6-31G(d,p results *in vacuo*). The blue color indicates the regions with the highest HOMO or LUMO density.

C1−C2 regions and the N1 and N2 atoms are the centers with the highest tendency to accept electrons from electron rich species.

The quantum chemical parameters describing the reactivity of the studied molecule are reported in Table 1. The energy of the HOMO (E_{HOMO}) provides information about the tendency of the molecule to donate electrons. The molecule with the highest E_{HOMO} value often has the highest tendency to donate electrons [15]. The E_{HOMO} values shown in table 1 suggest that the tendency to donate electrons is in the order; MPQ < PPQ < MHPQ < PHPQ < MM$_t$HPQ. The E_{LUMO} values provide information on the tendency of the molecule to accept electrons. A low E_{LUMO} value suggests that the molecule has a high tendency to accept electrons from an electron rich species. The order of the E_{LUMO} values for the studied molecules is such that MM$_t$HPQ < MPQ < PPQ < MHPQ < PHPQ. The ΔE values (i.e., the energy difference between E_{HOMO} and E_{LUMO}) provide information about the reactivity of molecules. The smaller ΔE value corresponds to high reactivity and show a high tendency to adsorb onto the metal surface [16]. The values of ΔE for the studied compounds suggests that the reactivity tendency follows the order; MPQ < PPQ < MM$_t$HPQ < MHPQ < PHPQ, indicating that PHPQ has the least tendency to reactivity.

Table 1. Quantum chemical parameters[a] for the calculated quinoxaline derivatives

Structure	E_{HOMO}	E_{LUMO}	ΔE	η	σ	$\mu(D)$	MV	logP	pol	Ave. IE[b]
B3LYP/6-31G(d) results *in vacuo* for neutral species										
MPQ	-6.28	-1.81	4.47	2.24	0.45	0.45	240	3.22	60	68.33
PPQ	-6.06	-1.89	4.17	2.09	0.48	0.38	305	4.62	65	72.08
MHPQ	-5.78	-2.12	3.66	1.83	0.55	1.62	245	2.83	60	53.00
PHPQ	-5.74	-2.16	3.58	1.79	0.56	1.75	311	4.25	66	63.70
MM$_t$HPQ	-5.57	-1.72	3.85	1.93	0.52	2.61	274	2.71	63	81.48
B3LYP/6-311G(d) results *in vacuo* for neutral species										
MPQ	-6.53	-2.06	4.47	2.24	0.45	0.46	239	3.22	60	68.33
PPQ	-6.31	-2.14	4.17	2.09	0.48	0.43	305	4.62	65	72.08
MHPQ	-6.05	-2.36	3.69	1.85	0.54	1.61	245	2.83	60	53.00
PHPQ	-6.00	-2.40	3.60	1.80	0.56	1.75	310	4.23	66	63.70
MM$_t$HPQ	-5.80	-1.97	3.83	1.92	0.52	2.74	273	2.71	63	81.48
B3LYP/6-31+G(d) results *in vacuo* for neutral species										
MPQ	-6.58	-2.14	4.44	2.22	0.45	0.51	240	3.22	60	68.33
PPQ	-6.36	-2.22	4.14	2.07	0.48	0.41	305	4.62	65	72.08
MHPQ	-6.14	-2.45	3.69	1.85	0.54	1.65	246	2.83	60	53.00
PHPQ	-6.10	-2.48	3.62	1.81	0.55	1.79	311	4.23	66	63.70
MM$_t$HPQ	-5.92	-2.07	3.85	1.93	0.52	2.69	273	2.71	63	81.48
B3LYP/6-31G(d) results *in vacuo* for protonated species										
MPQ-p	-10.42	-6.75	3.67	1.84	0.54	2.97	242	2.85	60	68.33
PPQ-p	-9.51	-6.57	2.94	1.47	0.68	5.29	307	4.25	66	72.08
MHPQ-p	-9.12	-6.94	2.18	1.09	0.92	7.32	248	2.46	61	53.00
PHPQ-p	-8.92	-6.72	2.2	1.10	0.91	6.45	311	4.23	66	63.70
MM$_t$HPQ-p	-9.24	-6.46	2.78	1.39	0.72	2.91	276	2.34	63	81.48
B3LYP/6-31G(d) results in water solution for neutral species										
MPQ-aq	-6.45	-2.07	4.38	2.19	0.46	0.67	240	3.22	60	68.33
PPQ-aq [c]							305	4.62	65	72.08
MHPQ-aq	-6.02	-2.26	3.76	1.88	0.53	2.26	246	2.83	60	53.00
PHPQ-aq [c]							311	4.23	66	63.70
MM$_t$HPQ-aq	-5.73	-2.03	3.7	1.85	0.54	3.49	273	2.71	63	81.48

[a] ΔE is the energy difference between E_{HOMO} and E_{LUMO}; μ is the dipole moment in Debye; MV is the molecular volume in Å^3; pol is the polarization; η is the hardness; σ is the global softness; HBC is the hydrogen bond donor acceptor capability. All energy values are in eV.

[b] the average experimental percent inhibition efficiency (ave %IE) was estimated from table 9 in [3] for the case in which no KCl, KBr and KI was added.

[c] On optimization in water solution, the calculation stop before convergence is achieve

The molecular volume (MV) provides information about the surface coverage of the metal by the inhibitor molecule. The compound that has large MV value has the highest surface coverage and hence might give greater protection of the metal surface. The MV values of the studied molecules are in the order; MPQ < MHPQ < MM$_t$HPQ < PPQ < PHPQ.

Table 2. Mulliken atomic charges (*e*) on the selected atoms of the studied compounds (B3LYP/6-31G(d,p) results *in vacuo*)

Atom	MPQ	PPQ	MHPQ	PHPQ	MM$_t$HPQ
C1	0.183	0.190	0.277	0.280	0.183
C2	0.282	0.190	0.282	0.181	0.280
N3	−0.524	−0.533	−0.521	−0.523	−0.525
C4	0.272	0.281	0.268	0.272	0.271
C5	−0.154	−0.156	−0.153	−0.154	−0.155
C6	−0.136	−0.136	−0.135	−0.135	−0.137
C7	−0.136	−0.136	−0.136	−0.136	−0.136
C8	−0.156	−0.156	−0.161	−0.160	−0.157
C9	0.285	0.281	0.318	0.312	0.286
N10	−0.536	−0.533	−0.662	−0.654	−0.540
C11	0.092	0.084	0.045	0.042	0.087
C12	−0.145	−0.148	0.307	0.304	−0.157
O12			−0.653	−0.656	
C13	−0.137	−0.138	−0.165	−0.166	−0.177
C14	−0.123	−0.123	−0.127	−0.127	0.311
O14					−0.648
C15	−0.137	−0.137	−0.146	−0.145	0.340
O15					−0.553
C16	−0.166	−0.153	−0.190	−0.183	−0.248
C17	−0.525	0.084	−0.531	0.077	−0.526
C18		−0.148		−0.147	
C19		−0.138		−0.137	
C20		−0.123		−0.123	
C21		−0.137		−0.136	
C22		−0.153		−0.148	

3.2. Selectivity/reactivity parameters

Selectivity parameters indicate the regions (of a molecule) that are likely to interact with the metal surface. These parameters include the Mulliken atomic charges, the condensed Fukui functions, and the local softness indices. The atom with the highest negative partial atomic charge interacts strongly with the metal surface through a donor-acceptor type of interaction because it represents the site with the highest electron density [17]. Table 2 reports the Mulliken atomic charges on the atoms of

the studied compounds. In all the compounds, the highest negative charge is on the heteroatoms mainly because these atoms have lone pair of electrons. These lone pair of electrons could be donated to the vacant *s* or partially filled *d* orbitals of the metal and thereby facilitate the adsorption of the inhibitor on the metal surface. MHPQ, PHPQ and MM$_t$HPQ have more heteroatoms than MPQ and PPQ because of the presence of the O atoms in these compounds. Therefore, MHPQ, PHPQ and MM$_t$HPQ have higher charge density and would interact with the metal surface at more sites than MPQ and PPQ. MM$_t$HPQ with the highest number of heteroatoms has the highest sites for adsorption onto the metal surface. This many explain the preference of MM$_t$HPQ as corrosion inhibitor among the compounds as reported earlier in literature [4].

Table 3. Local selectivity parameters (i.e., the condensed Fukui functions and the local softness parameters) for the studied quinoxaline derivatives (B3LYP/6-31G(d,p) results *in vacuo*).

a) The condensed Fukui Functions on the selected atoms of the studied compounds

Atom	MPQ		PPQ		MHPQ		PHPQ		MM$_t$HPQ	
	$|f^-|$	$|f^+|$	$|f^-|$	$|f^+|$	$|f^-|$	$|f^+|$	$|f^-|$	$|f^+|$	$|f^-|$	$|f^+|$
C1	0.034	0.048	0.027	0.034	0.020	0.059	0.02	0.047	0.018	0.046
C2	0.018	0.020	0.027	0.034	0.018	0.019	0.025	0.028	0.016	0.022
N3	0.035	0.078	0.021	0.081	0.028	0.078	0.023	0.080	0.027	0.080
C4	0.021	0.013	0.023	0.008	0.019	0.009	0.019	0.007	0.017	0.011
C5	0.024	0.033	0.011	0.034	0.011	0.032	0.009	0.033	0.012	0.034
C6	0.039	0.019	0.019	0.013	0.024	0.018	0.018	0.014	0.025	0.018
C7	0.006	0.009	0.019	0.013	0.010	0.010	0.013	0.012	0.006	0.010
C8	0.035	0.037	0.011	0.034	0.015	0.035	0.011	0.033	0.019	0.037
C9	0.021	0.005	0.023	0.008	0.019	0.008	0.020	0.009	0.013	0.005
N10	0.028	0.082	0.021	0.081	0.003	0.057	0.000	0.058	0.016	0.082
C11	0.014	0.002	0.005	0.004	0.044	0.009	0.037	0.007	0.023	0.005
C12	0.027	0.011	0.016	0.006	0.034	0.018	0.029	0.014	0.033	0.010
O12					0.104	0.029	0.085	0.025		
C13	0.010	0.004	0.010	0.002	0.031	0.010	0.021	0.008	0.023	0.005
C14	0.040	0.023	0.028	0.015	0.016	0.020	0.017	0.015	0.040	0.033
O14									0.085	0.029
C15	0.012	0.004	0.005	0.003	0.049	0.004	0.031	0.003	0.049	0.019
O15									0.038	0.011
C16	0.026	0.012	0.013	0.006	0.011	0.017	0.012	0.011	0.029	0.017
C17	0.011	0.170	0.005	0.004	0.013	0.011	0.006	0.007	0.011	0.009
C18			0.016	0.006			0.009	0.004		
C19			0.010	0.002			0.006	0.002		
C20			0.028	0.015			0.017	0.012		
C21			0.005	0.003			0.004	0.002		
C22			0.013	0.006			0.001	0.001		

b) Local softness parameters on the selected atoms of the studied compounds

Atom	MPQ		PPQ		MHPQ		PHPQ		MM$_t$HPQ	
	$\lvert s^-\rvert$	$\lvert s^+\rvert$	$\lvert s^-\rvert$	$\lvert s^+\rvert$	$\lvert s^-\rvert$	$\lvert s^+\rvert$	$\lvert s^-\rvert$	$\lvert s^+\rvert$	$\lvert s^-\rvert$	$\lvert s^+\rvert$
C1	0.015	0.022	0.013	0.016	0.011	0.032	0.011	0.026	0.009	0.024
C2	0.008	0.009	0.013	0.016	0.010	0.010	0.014	0.016	0.008	0.011
N3	0.016	0.035	0.010	0.039	0.015	0.043	0.013	0.045	0.014	0.042
C4	0.009	0.006	0.011	0.004	0.010	0.005	0.011	0.004	0.009	0.006
C5	0.011	0.015	0.005	0.016	0.006	0.018	0.005	0.018	0.006	0.018
C6	0.018	0.009	0.009	0.006	0.013	0.010	0.010	0.008	0.013	0.009
C7	0.003	0.004	0.009	0.006	0.006	0.006	0.007	0.007	0.003	0.005
C8	0.016	0.017	0.005	0.016	0.008	0.019	0.006	0.018	0.010	0.019
C9	0.009	0.002	0.011	0.004	0.010	0.004	0.011	0.005	0.007	0.003
N10	0.013	0.037	0.010	0.039	0.002	0.031	0.000	0.032	0.008	0.043
C11	0.006	9E04	0.002	0.002	0.024	0.005	0.021	0.004	0.012	0.003
C12	0.012	0.005	0.008	0.003	0.019	0.010	0.016	0.008	0.017	0.005
O12					0.057	0.016	0.048	0.014		
C13	0.005	0.002	0.005	0.001	0.017	0.006	0.012	0.004	0.012	0.003
C14	0.018	0.010	0.013	0.007	0.009	0.011	0.010	0.008	0.021	0.017
O14									0.044	0.015
C15	0.005	0.002	0.002	0.001	0.027	0.002	0.017	0.002	0.025	0.010
O15									0.020	0.006
C16	0.012	0.005	0.006	0.003	0.006	0.009	0.007	0.006	0.015	0.009
C17	0.005	0.077	0.002	0.002	0.007	0.006	0.003	0.004	0.006	0.005
C18			0.008	0.003			0.005	0.002		
C19			0.005				0.003	0.001		
C20			0.013	0.007			0.010	0.007		
C21			0.002	0.001			0.002	0.001		
C22			0.006	0.003						

The Fukui functions indicate the regions on the inhibitor molecule on which nucleophilic and electrophilic reactions are likely to occur. These functions are generally expressed using the finite difference approximation as follows [18]:

$$f^+ = q_{(N+1)} - q_N \qquad \text{for nucleophilic attack} \qquad (8)$$

$$f^- = q_N - q_{(N-1)} \qquad \text{for electrophilic attack} \qquad (9)$$

where $q_{(N+1)}$, q and $q_{(N-1)}$ are the charges of the atoms on the anionic, neutral and cationic systems respectively. The preferred site for nucleophilic attack is the atom in the molecule where the value of f^+ is the highest while the preferred site for electrophilic attack is the atom in the molecule where f^- has the highest value. The calculated values of the Fukui functions for the non-hydrogen atoms are reported in Table 3a. The value of f^+ is highest on N3 and N10 in all the compounds indicating that these atoms are likely to be engaged in a nucleophilic attack on the inhibitor. These results agree with the analysis of the LUMO which indicated that each N atom has an anti-bonding orbital and is therefore electron deficient. The value of f^- is highest on C1, C6, C8 and C14 in MPQ;

C1, C2, C14 and C20 in PPQ; C11, C12 and O12 in MHPQ and PHPQ; C14, O14 and C15 in MM$_t$HPQ. These results also correlate well with the analysis of the HOMO density discussed earlier.

The local reactivity of molecules is often analyzed in terms of the local softness index *s*, which is defined as the product of the Fukui function and the global softness, σ. It is expressed using the equation [19];

$$s = (f^+)^*\sigma \tag{10}$$

$$s = (f^-)^*\sigma \tag{11}$$

and the results, reported in Table 3b show that the local softness values predict similar sites for nucleophilic and electrophilic attack as the condensed Fukui functions.

3.3 Results of the calculations in vacuo for the protonated species

In aqueous acid environment, inhibitor molecules that have heteroatoms are likely to be protonated. Protonation is greater on N atoms than on O atoms because the former has the least tendency to hold on its lone pair of electrons while the later has the highest tendency. Since all the quinoxaline molecules have N atoms, they are all likely to be protonated in aqueous acid medium. The protonated species of the compounds also have a tendency to adsorb onto the metal surface, and therefore it is interesting to investigate their properties and compare them with the properties of the neutral species. Due to the symmetric nature of the molecular structure of PPQ only the protonation at N10 was investigated for other compounds (e.g., MPQ, and MM$_t$HPQ) the protonation at N3 and N10 was investigated separately to determine the preferred site for protonation. The preferred site for protonation was determined by comparing the total energy of the calculated protonated species for each compound. The species with the lowest total energy corresponded to the species with the preferred protonation site. The calculated protonated species for the quinoxaline compounds are shown in figure. 2. The results show that in MPQ and MM$_t$HPQ, the preferred site for protonation is N10 (i.e., the site closer to the phenyl substituent group). The discussion on protonated species in the next paragraphs concerns only the preferred protonated forms of the studied compounds.

An interesting quantity to consider is the extent of protonation because it is an indicator of the tendency of a given molecule to be protonated. The extent of protonation is measured by the proton affinity (PA). A high value of PA indicates that the molecule has a high tendency to be protonated. The calculated PA values (kcal/mol) for the quinoxaline protonated species is 64.333 for MPQ, 65.725 for PPQ, 58.031 for MHPQ, 62.047 for PHPQ and 68.782 for MM$_t$HPQ, which indicates that MPQ has the least tendency for protonation while MM$_t$HPQ has the highest tendency for protonation in aqueous acidic environment.

A comparison of the quantum chemical reactivity parameters for protonated species and the neutral species indicates the relative tendency of the two species to interact with the metal surface. The quantum chemical parameters of the protonated species are also reported in Table 1. E$_{HOMO}$ of the

protonated species is 3.18–4.80eV lower than that of the neutral species, indicating that the tendency of the protonated species to donate electrons to the metal surface is less than that of the neutral species. E_{LUMO} of the protonated species is 4.74–5.62eV lower than that of the neutral species indicating that protonation increases the electron accepting ability of the inhibitors. The dipole moment is always larger for the protonated species than for the neutral species, indicating that the interaction between the metal surface and the protonated species involves more electrostatic interactions than the interaction between the neutral species the metal surface. The logP values for the protonated species are always smaller than that of the corresponding neutral species, suggesting that the protonated species are less hydrophobic than the neutral species. The results obtained indicate that the corrosion inhibition effectiveness of neutral species is higher than that of protonated species.

3.4. Results of the calculations in water solution for the neutral species

The investigation of the molecular properties of corrosion inhibitors needs to take into consideration solvent effects because molecular properties of a given molecule may differ between aqueous solution (in which most electrochemical reactions are conducted) and *vacuum* medium. An interesting parameter to consider is the free energy of solvation (ΔG_{solv}) because it provides information on the extent of molecular solvation. Different compounds are affected to varying degrees by solvent molecules and the free energy of solvation provides information about the relative tendency of the inhibitors to remain in solution. A high ΔG_{solv} value for an inhibitor indicates that its molecules are highly solvated. Compounds that have great tendency to be solvated are often not good corrosion inhibitors because they interact more strongly with solvent molecules than with the metal surface [20]. The ΔG_{solv} values (kcal/mol) for the investigated quinoxaline compounds are −6.941 for MPQ, −8.401 for MHPQ, and −11.611 for MM$_t$HPQ, which indicates that the solvation energy decreases with the increase in the number of polar substituent groups.

A comparison of the molecular properties of the studied compounds between the results *in vacuo* and the results in water solution provide information about the influence of the solvent effects on the molecular properties. The values of the molecular properties in water solution, reported in Table 1, suggest that the E_{HOMO}, E_{LUMO} and the dipole moment values are not significantly different from the results *in vacuo*, implying that solvent effects have minimal influence on the molecular properties of quinoxaline derivatives.

3.5. Quantitative structure activity relationship (QSAR)

A combination of several quantum chemical parameters to form a composite index, which could be correlated to the experimental inhibition efficiency, often provides valuable information on the relationship between quantum chemical parameters and experimental inhibition efficiency (%IE). Usually, a correlation between quantum chemical parameters and the observed inhibition efficiency is investigated by means of quantitative structure activity relationship (QSAR) approach in which relevant mathematical equations are utilised to relate the quantum chemical parameter to the observed

inhibition efficiency of an inhibitor. The experimental determination of the inhibition efficiency of the studied quinoxalines has also confirmed that the adsorption of inhibitors follows Langmuir adsorption isotherm [4]. Therefore, it is reasonable to employ the linear and the non-linear mathematical models proposed by Lukovits *et al* [21, 22] in order to correlate the observed inhibition efficiency to the calculated quantum chemical parameters. The linear model has the form

$$IE_{theor} = Ax_i C_i + B \tag{12}$$

where A and B are the regression coefficients determined through regression analysis, x_i is a quantum chemical index characteristic of the molecule i, C_i is the experimental concentration of the inhibitor. The non-linear model has the form

$$IE_{theor} = \frac{(AX_i + B) * C_i}{1 + (AX_i + B) * C_i} * 100 \tag{13}$$

where A and B are constants obtained by regression analysis; X_i is a quantum chemical index characteristic for the molecule; C_i is the inhibitor concentration in mM.

E_{HOMO}, E_{LUMO}, pol (linear regression equation) E_{HOMO}, E_{LUMO}, pol (non-linear regression equation)
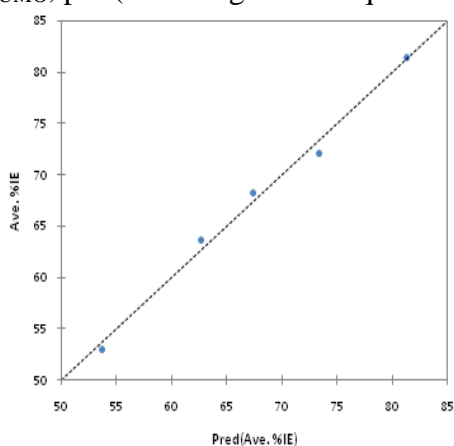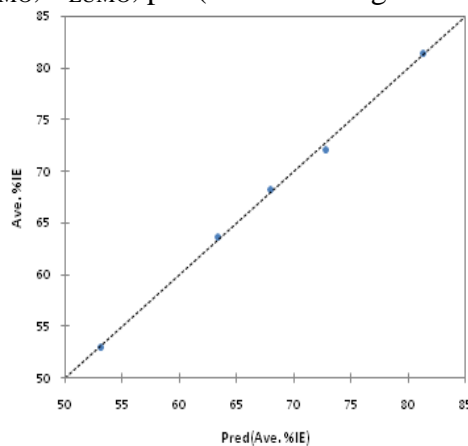
Figure 4. Representative plot of correlation between the theoretically estimated %IE and experimentally obtained %IE [The items above each plot indicates the quantum chemical parameters used to form the composite index. The quantum chemical properties are obtained from B3LYP/6-31G(d,p) results].

Equations (11) and (12) were utilized to correlate the composite index of the quantum chemical parameters with the experimental inhibition efficiency of the studied quinoxalines. The results show that an optimum of three quantum chemical parameters is sufficient to produce a good correlation with experimentally determined inhibition efficiency. Combinations of the quantum chemical parameters that provide the best correlation with experimental inhibition efficiencies are reported in Table 4

together with the equations for the prediction of theoretical inhibition efficiencies and the corresponding R^2, SSE and RMSE values.

Table 4. A pair of quantum chemical parameters utilized to derive the linear and the non-linear multiple regression equation that correlates the theoretically estimated and the experimentally determined inhibition efficiencies. The R^2 value, the SSE and the RMSE values are also reported. The quantum chemical parameters were obtained from the *in vacuo* results calculated using the B3LYP/6-31G(d) method.

Quantum parameters	Derived QSAR equation	R^2	SSE	RMSE
Linear model				
E_{HOMO}, E_{LUMO}, pol	%IE = 87.5*E_{HOMO}*C_i + 876.7*E_{LUMO}*C_i + 30.1*pol*C_i + 87.4	0.991	4.179	2.044
E_{HOMO}, E_{LUMO}, MV	%IE = 99.6*E_{HOMO}*C_i + 893.5*E_{LUMO}*C_i + 2.5*MV*C_i + 166.1	0.981	8.465	2.910
ΔE, μ, MV	%IE = 722.6*ΔE*C_i + 233.8*μ*C_i + 3.8*MV*C_i -185.3	0.980	8.764	2.960
E_{HOMO}, E_{LUMO}, logP	%IE = 281.7*E_{HOMO}*C_i + 978.4*E_{LUMO}*C_i + 97.5*logP*C_i + 260.5	0.967	14.567	3.817
E_{HOMO}, E_{LUMO}, μ	%IE = 559.5*E_{HOMO}*C_i + 906.0*E_{LUMO}*C_i -119.2*μ*Ci + 380.5	0.823	78.278	8.848
Non-linear model				
E_{HOMO}, E_{LUMO}, pol	%IE = (((30.2*E_{HOMO}+ 101.9*E_{LUMO} + 2.1*pol + 280.8)* C_i)/ (1+ (30.2*E_{HOMO} + 101.9*E_{LUMO} + 2.1*pol+ 280.8)* C_i))*100	0.998	0.766	0.875
E_{HOMO}, E_{LUMO}, MV	%IE = (((29.7*E_{HOMO} + 102.8*E_{LUMO} + 0.2*MV + 362.4)* C_i)/ (1+ (29.7*E_{HOMO} + 102.8*E_{LUMO} + 0.2*MV+ 362.4)* C_i))*100	0.995	2.176	1.475
ΔE, μ, MV	%IE = (((65.0*ΔE+ 24.1*μ + 0.3*MV - 322.6)* C_i)/ (1+ (65.0*ΔE+ 24.1*μ + 0.3*MV - 322.6)* C_i))*100	0.923	34.716	5.892
E_{HOMO}, E_{LUMO}, logP	%IE = (((43.4*E_{HOMO} + 109.8*E_{LUMO} + 8.2*logP + 479.5)* C_i)/ (1+ (43.4*E_{HOMO} + 109.8*E_{LUMO} + 8.2*logP + 479.5)* C_i))*100	0.989	4.776	2.186

The best equation resulting from both the linear and the non-linear multiple regression equations (plotted in figure 4) is a result of the combination of E_{HOMO}, E_{LUMO} and polarization (pol) parameters. The linear equation resulting from such combination is of the form;

$$IE_{theo} = 87.5*E_{HOMO}*C_i + 876.7*E_{LUMO}*C_i + 30.1*pol*C_i + 87.4 \qquad (14)$$

with R^2 = 0.991, SSE = 4.179 and RMSE = 2.044

The equation suggests that a high E_{HOMO}, E_{LUMO} and a molecular polarization results in greater inhibition efficiency. The non-linear equation resulting from the combination of the of E_{HOMO}, E_{LUMO} and polarization (pol) parameters has the form;

$$\%IE = (((30.2*E_{HOMO}+ 101.9*E_{LUMO} + 2.1*pol + 280.8)*C_i)/ (1+ (30.2*E_{HOMO} + 101.9*E_{LUMO} + 2.1*pol+ 280.8)*C_i))*100 \tag{15}$$

with $R^2 = 0.998$, SSE $= 0.766$ and RMSE $= 0.875$.

Since for most of the equations in Table 4 the values of R^2 are reasonably high (> 0.900) while the SSE and RMSE values are reasonably small, it is reasonable to infer that the combination of three quantum chemical parameters provides a good correlation between quantum chemical parameters and experimentally determined inhibition efficiency of the studied quinoxaline inhibitors.

R^2 is the coefficient of determination, and *SSE* and RMSE are defined as

$$SSE = \sqrt{\sum_{i=1}^{n}\left(IE_{pred} - IE_{\exp}\right)^2}$$

$$RMSE = \sqrt{\frac{1}{n}\sum_{j=1}^{n}\left(IE_{pred} - IE_{\exp}\right)^2}$$

where IE_{pred} is the predicted inhibition efficiency and IE_{exp} is the experimental determined inhibition efficiency, n is the number of observations (compounds) considered

3.6. The adsorption of quinoxalines on copper surface

The adsorption of quinoxaline molecules on the metal surface (e.g., mild steel or copper surface as indicated in [4]) involves both physical and chemical adsorption. The protonated species are physically adsorbed on the metal surface because of their electrostatic interactions with the already adsorbed anions (e.g., Cl^- or SO_4^-, [23]). The neutral species adsorb onto the metal surface both physically and chemically. Physical adsorption involves the electrostatic attraction of the inhibitor onto the metal surface whereas the chemical adsorption involves the donation of electrons by the inhibitor molecule to the vacant *s* or *d* orbital of the metal atoms. Chemical adsorption may also involve the metal atom donating some of its electrons in the occupied *d* orbitals to the LUMO of the inhibitor molecules in a back-donation mechanism. In the case of Cu surface, the inhibitor⋯metal interaction mechanism may be modelled by placing a Cu atom in the vicinity of the electron-donor centres (i.e., chelating or active adsorption sites) and optimizing the resulting geometry. This consideration assumes that the metal atom chelation ability with the inhibitor is related to the corrosion inhibition efficiency [3, 24–29]. The optimized complexes are then utilized to determine the preferred geometries and estimate the binding energies, the inhibitor⋯Cu separation distances, and the charge transfer

mechanism involved between the inhibitor and the Cu atom. Although the inhibitor···Cu interaction energy obtained from this model does not reflect the real interaction energy between the inhibitor and the Cu surface (which contains many Cu atoms), it is nevertheless a good model for qualitative analysis of the type of interactions involved and a good indication of the inhibitor···Cu interaction strength for different electron donor sites (active adsorption sites) on the inhibitor molecule.

The optimised inhibitor···Cu complexes are shown in figure. 5 together with the relative energy of the complexes for cases where the Cu atom has more than one binding sites on the inhibitor molecule. In complexes of structure MPQ and MM$_t$HPQ, the preferred geometries (i.e., MPQ-Cu(1) and MM$_t$HPQ-Cu(2)) are those in which the Cu atom is in tri-dentate mode to the active adsorption sites of the inhibitor molecule. However, this preference is not observed in the complexes of structures MHPQ and PHPQ because, the tri-dentate geometries in structures MHPQ and PHPQ results from the disruption of the N10···H12-O intramolecular hydrogen bond (IHB). Therefore, in MHPQ and PHPQ, stabilisation of the complexes is determined by both the presence of the copper atom in the vicinity of the adsorption sites as well as the presence of IHB.

complex	PPQ-Cu	
complex	MPQ-Cu(1)	MPQ-Cu(2)
relative energy	0.000	12.280
complex	MHPQ-Cu(1)	MHPQ-Cu(2)
relative energy	2.259	0.000
complex	PHPQ-Cu(1)	PHPQ-Cu(2)
relative energy	10.737	0.000

complex	MM$_t$HPQ(1)	MM$_t$HPQ-Cu(2)	MM$_t$HPQ-Cu(3)	MM$_t$HPQ-Cu(4)
relative energy	36.402	0.000	12.820	35.040
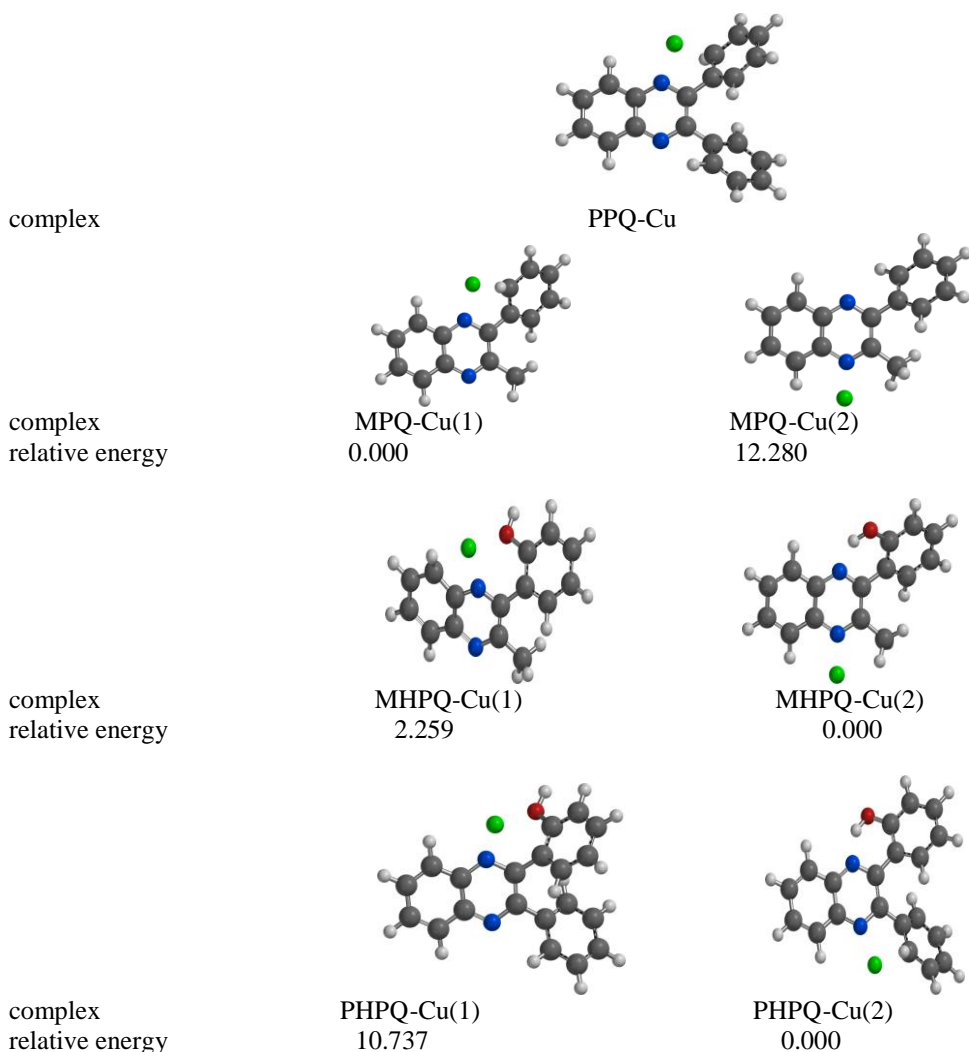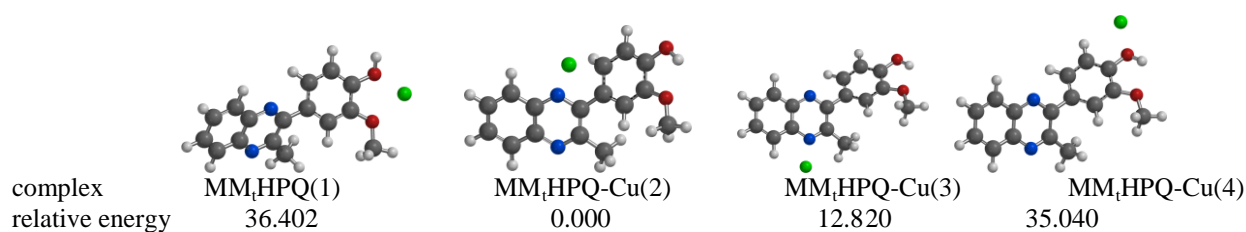
Figure 5. The *in vacuo* optimized quinoxaline···Cu complexes using the B3LYP/6-31G(d,p) method. The relative energy (kcal/mol) for different complexes of the same inhibitor molecule is reported below the structures. The total energy (kcal/mol) of the lowest-energy complex for each structure in which there are more than one complexes is -1461213.74 for MPQ-Cu(1), -1508406.01 for MHPQ-Cu, -1628735.48 for PHPQ-Cu(2) and -1580278.12 for MM$_t$HPQ-Cu(2)

The binding energies and the deformation energies for the complexes are reported in Table 5. A comparison of the binding energies of MPQ···Cu(2), MHPQ···Cu(2) and MM$_t$HPQ···Cu(3), where the Cu atom is in mono-dentate mode to the N atom, suggests that the Cu atom affinity is similar for the three complexes, which implies that the affinity of the Cu atom is not determined by the substituent group on the quinoxaline moiety.

Table 5. The inhibitor-Cu interaction energy (E_{inter}, kcal/mol), deformation energy (E_{def}, kcal/mol) and binding energy (E_b, kcal/mol) estimated from the energies of the complexes and the corresponding energies of the isolated inhibitor ($_{inh, isol}$) and Cu. B3LYP/6-31G(d) results *in vacuo*.

Complex	$E_{complex}$ (hartree)	$E_{inh, isol}$ (hartree)	$E_{Cu, isol}$ (hartree)	$E_{inhi+Cu, isol}$ (hartree)	$E_{inh, complex}$ (hartree)	E_{def} (kcal/mol)	E_{inter} (kcal/mol)	E_b (kcal/mol)
MPQ···Cu(1)	-2328.59407	-688.342131	-1640.17418	-2328.51631	-688.323235	-11.857	-48.795	-36.937
MPQ···Cu(2)	-2328.57450	-688.342131	-1640.17418	-2328.51631	-688.340203	-1.210	-36.514	-35.304
PPQ···Cu	-2520.33027	-880.077981	-1640.17418	-2520.25216	-880.060619	-10.895	-49.014	-38.119
MHPQ···Cu(1)	-2403.79620	-763.557305	-1640.17418	-2403.73149	-763.523981	-20.911	-40.609	-19.698
MHPQ···Cu(2)	-2403.79980	-763.567653	-1640.17418	-2403.74183	-763.565159	-1.565	-36.375	-34.810
PHPQ···Cu(1)	-2595.54005	-955.289375	-1640.17418	-2595.46356	-955.273512	-9.954	-48.001	-38.047
PHPQ···Cu(2)	-2595.55716	-955.303127	-1640.17418	-2595.47731	-955.286712	-10.301	-50.109	-39.808
MM$_t$HPQ···Cu(1)	-2518.27747	-878.075528	-1640.17418	-2518.24971	-878.073123	-1.509	-17.421	-15.912
MM$_t$HPQ···Cu(2)	-2518.33548	-878.082822	-1640.17418	-2518.25700	-878.064124	-11.733	-49.246	-37.513
MM$_t$HPQ···Cu(3)	-2518.31505	-878.082822	-1640.17418	-2518.25700	-878.081053	-1.110	-36.426	-35.316
MM$_t$HPQ···Cu(4)	-2518.27964	-878.082822	-1640.17418	-2518.25700	-878.081281	-0.968	-14.206	-13.239

In MM$_t$HPQ···Cu(1), the Cu atom is in a bidentate mode between O14 and O15. A comparison of MM$_t$HPQ···Cu(1) and MM$_t$HPQ···Cu(4) suggests that the Cu affinity is 2.673 kcal/mol greater when it binds to two O atoms simultaneously than when it binds to one O atom. In PPQ···Cu, MPQ···Cu(1) and PHPQ···Cu, the Cu atom is in a tri-dentate mode.

Table 6 reports the inhibitor···Cu distance separation, the spin density and the electronic configuration of Cu atom in the isolated state and in the various complexes. The spin density and the electronic configuration of the isolated Cu atom indicate that there are four unpaired electrons in the 3d orbitals with the same spin orientation. Upon formation of the inhibitor···Cu complexes, the spin density on Cu atom decreases while the electronic configuration of Cu show those 3d orbitals have an increase in electron occupancy, suggesting that, while interacting with the metal atom, the inhibitor molecule has donated electrons to the partially filled 3d orbital of the metal atom. The decrease in the spin density suggests that the added electrons have opposite spin to the spin of the unpaired electron that was present in the Cu atom. The transfer of negative charge (electrons) from the inhibitor molecule to the metal surface amounts to adsorption of the inhibitor molecule on the metal surface by the formation of a chemical bond (i.e., chemisorption process). The spin density and the electronic configuration of the Cu atom depend also to some extent on the coordination structure of the complexes.
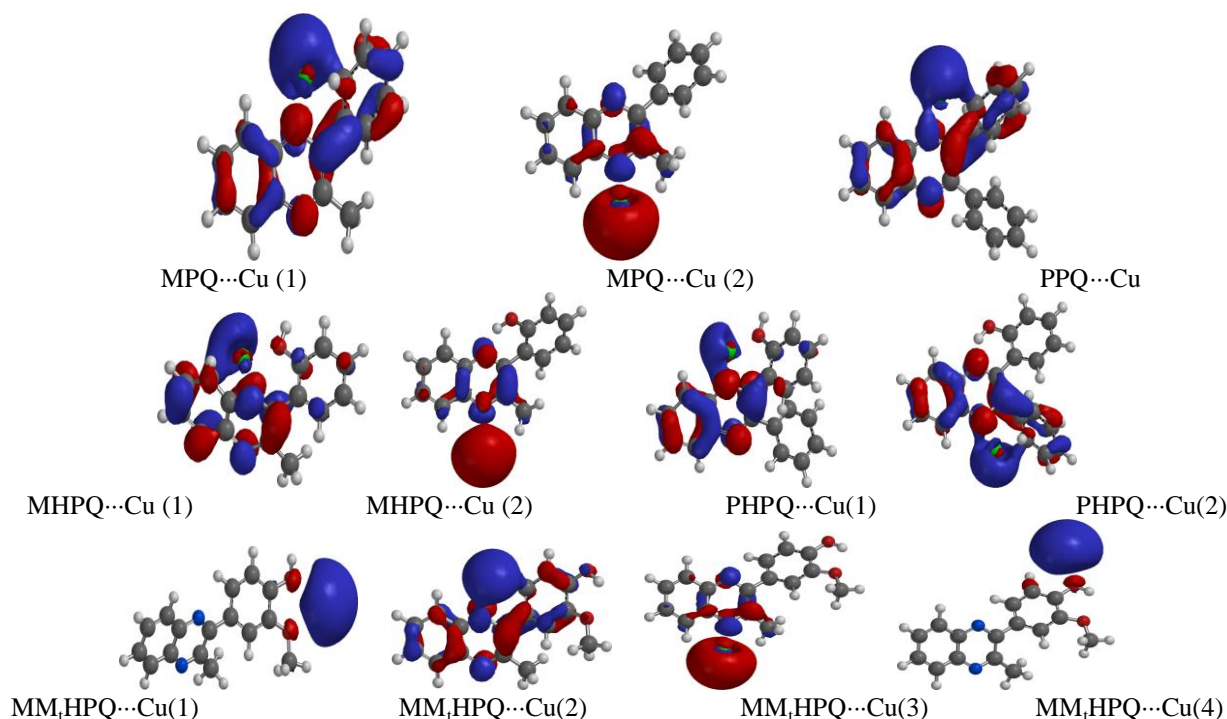
Figure 6. The single occupied molecular orbital (SOMO) for the calculated complexes of quinoxaline derivatives and Cu atom (B3LYP/6-31G(d) results *in vacuo*).

To better understand the nature of the bonding between the inhibitor and the metal atom, it is important to analyze the occupied molecular orbital of the isolated inhibitor molecule and of the corresponding inhibitor···Cu complex. Figure 6 shows the single occupied molecular orbital (SOMO) for each complex. Few examples suffice to illustrate the trend: in PPQ···Cu, MPQ···Cu(1) and MM$_t$HPQ···Cu(2), the electron density of the SOMO is shared by N10, C11, C12 and Cu atoms; in MPQ···Cu(2), MM$_t$HPQ···Cu(1), MM$_t$HPQ···Cu(3) and MM$_t$HPQ···Cu(4), it is strongly localised on the Cu atom, suggesting that there is weak interaction between the inhibitor molecule and the Cu atom.

Table 6. The inhibitor···Cu separation distances (Å), spin density and electronic configuration of the Cu atom in the complexes [a].

Complex	Bond type	Inhibitor···Cu separation distance	Spin density of Cu in the complex	Electronic configuration of Cu in the complex
MPQ···Cu(1)	N10·····Cu	1.897	0.381699	[core]4S(0.62)3d(9.59)4p(0.11)
	C11·····Cu	2.410		
	C12·····Cu	1.969		
MPQ···Cu(2)	N3·····Cu	1.836	0.692748	[core]4S(1.08)3d(9.55)4p(0.10)5S(0.01)
PPQ···Cu	N10·····Cu	1.897	0.350895	[core]4S(0.60)3d(9.59)4p(0.11)
	C11·····Cu	2.372		
	C12·····Cu	1.968		
MHPQ···Cu(1)	C8·····Cu	2.045	0.257125	[core]4S(0.55)3d(9.56)4p(0.09)
	C9·····Cu	2.090		
	N10·····Cu	2.010		
	O12·····Cu	1.990		
MHPQ···Cu(2)	N3·····Cu	1.832	0.624736	[core]4S(1.02)3d(9.55)4p(0.09)5S(0.01)
PHPQ···Cu(1)	N10·····Cu	1.802	0.161902	[core]4S(0.60)3d(9.56)4p(0.09)
	C1·····Cu	2.375		
	O12·····Cu	1.906		
PHPQ···Cu(2)	N3·····Cu	1.893	0.290703	[core]4S(0.56)3d(9.60)4p(0.10)
	C18·····Cu	2.334		
	C19·····Cu	1.968		
MM$_t$HPQ···Cu(1)	O14·····Cu	1.946	0.928438	[core]4S(1.43)3d(9.47)4p(0.09)
	O15·····Cu	2.305		
MM$_t$HPQ···Cu(2)	N10·····Cu	1.898	0.377881	[core]4S(0.62)3d(9.59)4p(0.11)
	C11·····Cu	2.403		
	C12·····Cu	1.968		
MM$_t$HPQ···Cu(3)	N3·····Cu	1.840	0.724735	[core]4S(1.11)3d(9.56)4p(0.10)5S(0.01)
MM$_t$HPQ···Cu(4)	O14·····Cu	1.933	0.941114	[core]4S(1.47)3d(9.46)4p(0.06)

[a], for the isolated Cu atom, the spin density is 1 and the electronic configuration is [core]4S(0.98)3d(4.02)

4. CONCLUSIONS

DFT studies on the geometries of selected quinoxaline derivatives were performed to obtain their molecular reactivity and selectivity parameters and to correlate some of the parameters to the experimentally determined inhibition efficiencies. The interaction mechanism between the inhibitors and Cu atom was also investigated to understand the nature of bonding.

- The results confirm that all the quinoxaline derivatives have high corrosion inhibition potential. MM$_t$HPQ has the highest potential to adsorb on the metal surface because it has the highest number of electron donor centers.

- Some of the quantum chemical parameters correlate well with the experimentally determined inhibition efficiencies of the studied quinoxaline inhibitors.

- The closeness of the electron donor centers in the selected quinoxaline derivatives also enhances the adsorption of the inhibitor on the metal surface because a single metal atom can receive electrons from two or more donor centers simultaneously.

- The preferred complexes are those in which the Cu atom is in multi-dentate mode to the studied inhibitor molecules.

References

1. S.S. Abdel-Rehim, K.F Khaled, N.A Al-Mobarak, *Arabian. J. Chem.*, 4 (2011) 333.
2. N.O. Obi-Egbedi, I.B. Obot, Mohammad I. El-Khaiary, *J. Mol. Struct.*, 1002 (2011) 86.
3. E. E. Ebenso, T. Arslan, F. Kandemirli, I. N. Caner, I. Love, *Int. J. Quantum Chem.*, 110 (2010) 1003.
4. S. Chitra, K. Parameswari, M.Vidhya, M. Kalishwari, A. Selvaraj, *Int. J. Electrochem. Sci.*, 6 (2011) 4593.
5. A.D. Becke, *J. Chem. Phys.*, 98 (1993) 5648.
6. P. Senet, *Chem. Phys. Lett.*, 275 (1997) 527.
7. P. Perez, R. Contreras, A. Vela, O. Tapia, *Chem. Phys. Lett.*, 269 (2007) 419.
8. P. Geerlings, F. De Proft, W. Langenaeker, *Chem. Rev.*, 103 (2003) 793.
9. L. Pauling, The Nature of the Chemical Bond (Coruell University Press, Ithaca, New York, (1960)
10. R.G. Parr, R. G. Pearson, *J. Am. Chem. Soc.*, 105(1983)7512.
11. G. Alagona, C. Ghio, *Phys. Chem. Chem. Phys.*, 11 (2009) 776.
12. Spartan,10 Wavefunction, Inc. Irvine, CA: Shao Y, Molnar LF, Jung Y, Kussmann J, Ochsenfeld C, Brown ST, Gilbert ATB, Slipehenko LV, Levehenko SV, O'Neill DP, DiStasio Jr. RA, Lochan RC, Wang T, Beran GJO, Besley NA, Herbert JM, Lin CY, Van Voorhis T, Chien SH, Sodt A, Steele RP, Rassolov VA, Maslen PE, Korambath PP, Adamson RD, Austin B, Baker J, Byrd EFC, Dachsel H, Doerksen RJ, Dreuw A, Dunietz BD, Dutoi AD, Furlani TR, Gwaltney SR, Heyden A, Hirata S, Hsu CP, Kedziora G, Khalliulin RZ, Klunzinger P, Lee AM, Lee MS, Liang WZ, Lotan I, Nair N, Peters B, Proynov EI, Pieniazek PA, Rhee YM, Ritchie J, Rosta E, Sherrill CD, Simmonett AC, Subotnik JE, Woodcock III HL, Zhang W, Bell AT, Chakraborty AK, Chipman DM, Keil FJ,

Warshel A, Hehre WJ, Schaefer HF, Kong J, krylov AI, Gill PMW, Head-Gordon M, *Phys. Chem. Chem. Phys.,* 8 (2010) 3172.
13. A.C. Chamberlin, C.J. Cramer, D. G. Truhlar, *J. Phys. Chem. B*., 112 (2008) 8651.
14. N.O. Eddy, *J. Adv. Res*., 2(2010)35.
15. G. Gece, S. Bilgic, *Corros. Sci*., 51 (2009) 1876.
16. M. K. Awad, M. R. Mustafa, M. M. Abo Elnga, *J. Mol.Struct.(Theochem)* 959 (2010) 66.
17. M.S. Masoud, M. K. Awad, Shaker, M.M.T. El-Tahawy, *Corros. Sci.,* 52 (2010) 2387.
18. P. Fuentealba, P. Perez, R. Contreras, *J. Chem. Phys.,* 113 (2000) 2544.
19. N.O. Eddy, B. I. Ita, *Int. J. Quant. Chem.,* 111 (2010) 3456.
20. L. S. Cammarata, G. Kazarian, P. A. Salterb, T. Welton, *Phys. Chem. Chem. Phys*., 3 (2001) 5192.
21. I. Lukovits, I. Bakó, A. Shaban, E. Kálmán, *Electrochim. Acta* 43 (1998) 131.
22. I. Lukovits, A. Shaban, E. Kalman, *Russian J. Electrochem*., 39 (2003) 177.
23. F. Bentiss, B. Mernari, M. Traisnel, H. Vezin, M. Lagrenée, *Corros. Sci*., 53 (2011) 487.
24. N. Kovačević, A. Kokalj, *J. Phys. Chem. C*., 115 (2011) 24189.
25. H. E. El Ashry, A. El Nemr, S. A. Esawy, S. Ragab, *Electrochim. Acta* 51(2006) 3957.
26. A. R. Katritzky, M. Karelson, V.S. Lobanov, *Chem. Rev*., 96 (1996) 1027.
27. N. O. Eddy, S. A. Odoemelam, *Pigment and Resin Technology* 38 (2009) 111.
28. N. O. Eddy, S. A. Odoemelam, A. O. Odiongenyi, *J. Appl. Electrochem*., 39 (2009) 849.
29. T. Arslan, F. Kandemirli, E. E. Ebenso, I. Love, H. Alemu, *Corros Sci*., 51(2009) 35.